Journal of Applied Fluid Mechanics, Vol. 17, No. 1, pp. 233-250, 2024.
Available online at www.jafmonline.net, ISSN 1735-3572, EISSN 1735-3645.
https://doi.org/10.47176/jafm.17.1.1867

3D Numerical Modeling and Geometry Optimization of an Oscillating Water Column Device in Sloshing Conditions Using Openfoam and Genetic Algorithms

S. S. Razavi†, R. Shafaghat, B. Alizadeh Kharkeshi and J. Eskandari

Sea-Based Energy Research group, Babol Noshirvani University of Technology, Babol, Mazandaran, 4714873113, Iran

†*Corresponding Author Email: rshafaghat@nit.ac.ir*

ABSTRACT

Among various types of wave energy converters, the oscillating water column (OWC) has attracted significant research attention. In this paper, a 1:10 scale OWC with dimensions of 100×100×160 cm, variable inlet height and draft was numerically studied. Based on the tests conducted, it was found that the wave amplitude in the range of Caspian Sea waves decreased with the increase of wave frequency, to the extent that at the sloshing frequency, the system efficiency dropped significantly. To solve this problem, changes in the geometry of the device were studied, and numerical simulations were performed at the highest frequency using OpenFOAM software. Using Reynolds-averaged Navier-Stokes (RANS) equations, numerical simulations were performed in 3D, two-phase, and turbulent flow conditions. Changing the geometry was initially investigated by adjusting the height of the OWC inlet duct, and then by adding an inlet at the different angles of 0, 20, and 40 degrees. The results showed that by increasing the height of the inlet by 10 cm while keeping the water depth and wave conditions constant, the maximum output power of the system increased by 54%. However, after the optimization of the inlet duct, it was found that the best angle for an inlet duct is 30°, compared to the case without an inlet, which increased the maximum output power by up to 13% and slightly reduced the sloshing by more than 50%.

Article History

Received March 8, 2023
Revised August 9, 2023
Accepted August 24, 2023
Available online November 1, 2023

Keywords:

Wave Energy
OWC
CFD
Sloshing
Performance

1. INTRODUCTION

Energy supply has always been a challenge and one of humanity's most basic needs. Over different eras, this demand has been met through coal and oil, but alternative methods have been considered due to these resources high pollution and limitations. Ocean waves are one of the most viable options for meeting a portion of human needs due to their high energy density. The oscillating water column (OWC) is particularly interesting among ocean waves' various energy conversion methods due to its simple structure, lack of moving parts, and low maintenance costs.

The OWC typically consists of a semi-submerged rectangular prism structure. The alternating inflow and outflow of seawater increases and decreases air pressure and flow rate inside the chamber relative to the outside. As a result, this difference creates airflow, and the energy of the sea waves is converted into electricity using a turbine and generator.

A 1:36 scale 3D model of an OWC under regular and irregular waves using the boundary element method in the period range of 0.8 to 3.2 seconds has been studied (Delauré & Lewis, 2003). The results showed that the depth of the water column, the thickness of the front wall, and the length of the OWC are effective in the system's performance.

The two-dimensional effects of front wall thickness and water depth on the performance of an OWC using Fluent software has been investigated (Horko, 2007). The numerical results were also validated using experimental tests on a system with a scale of 1:12.5. The system, which was investigated along the width of the water column and had a length of 0.03 meters, had dimensions of 0.64 meters in length and 1.37 meters in width, with a groove-shaped orifice. According to the results, a front wall with a thickness of 0.04 meters and a water depth of 1 meter had the maximum performance.

NOMENCLATURE

Greek symbols

α	sloshing angle
α_L	scale factor
ε (%)	efficiency
η	free surface fluctuations
λ	wavelength
μ	dynamic viscosity
μ_t	field turbulence coefficient
ρ	density
ω	angular frequency
Θ	inlet angle

Symbols

A	range of fluctuations
A	OWC length
B	OWC height
C	release speed
C	wave velocity
c_g	group speed of the wave
D	orifice diameter
D	draft depth
f_i	volumetric forces
f	attenuation equations in x direction
f	attenuation equations in z direction
E_I	collision energy
g	acceleration of gravity
H	wave height
H	depth of water
k	wave number
L	OWC width
$\dot{m}$	air mass flow rate
O	OWC inlet height
P	pressure
P_{out}	extractable power
P_{wave}	impact wave power
P_τ	kinetic energy production power due to turbulence shear stress
Q	volume flow rate of air
S	slope of the slashing line
T	wave period
t	time
u_i	average speed in three directions
V_{gate}	volume of water inside the valve
V_{OWC}	volume of water inside the fluctuating column of water
$V_{relative}$	dimensionless number of volume ratio
w	velocity in z-direction
Y_G	water height determined by oscilloscope
Δ	length of the hinged wave generator

The effects of wave impact and geometric parameters on the performance of an OWC have been numerically investigated (Liu et al., 2010). Four different models were studied in periods ranging from 2.5 to 8 seconds. The results showed that water depth, front wall thickness, and depth of the air chamber are influential geometric parameters affecting the performance of the OWC. Additionally, the study found that a water depth of 2.5 meters and an OWC width of 1.5 meters perform the best at a period of 4.5 seconds, compared to widths of 3 and 6 meters.

The effect of different wave conditions, the depth of the water, and the thickness of the front chamber wall on the performance of an OWC system have been studied (Zhang et al., 2012). It was found that changes in the thickness of the front chamber wall can influence the vortex generation pattern, and an increased energy dissipation rate due to changes in the thickness of the front chamber wall can reduce the efficiency of the OWC. In addition, the pressure and free surface oscillations have a phase difference of π/2, and increasing the diameter of the orifice reduces the pressure inside the chamber and increases the efficiency of the OWC.

The performance of the OWC by creating a step on the sea floor with different dimensions relative to the length of the converter has been investigated (Rezanejad et al., 2013). The results showed that a significant increase in system performance could be achieved by reducing the water depth inside the OWC using a step. Furthermore, suppose the length of the step is designed to be close to one-quarter of the input wavelength. In that case, the net force resulting from wave impact on the OWC will be maximized, leading to an increase in oscillatory motion and improved OWC efficiency.

The reflection coefficient, frequency, amplification, and relationship with geometric parameters have been evaluated (Çelik & Altunkaynak, 2020). The results showed that the system performance is optimal at the resonant frequency.

Changes in the front wall's length, width, and anglehave been made to achieve the best structure (Mahnamfar & Altunkaynak, 2017). After optimization, the system efficiency increased by 10.81%. The highest efficiency was achieved at a water depth of 50 cm, an inlet height of 41 cm, and a width of 75 cm.

The chamber's geometry has been investigated to achieve the best performance of the OWC (Teixeira et al., 2013). It was found that a water depth of 10 meters, a chamber with a draft depth of 2.5 meters, and a length and width of 10 meters provide the highest pneumatic power. The effect of changing the inlet geometry on the OWC performance has been investigated to evaluate the impact of the front wall angle between -45 to 180 degrees (Bouali & Larbi, 2013). Optimal geometry and dimensions were studied to achieve the best OWC performance, with the front wall's angle being a critical factor in the system's efficiency. The best performance was observed at a zero-degree angle.

The effect of orifice area on OWC performance has been studied using OpenFOAM software (Simonetti et al., 2015). After validating the numerical results with experimental tests and optimizing the orifice-to-chamber

surface area ratio, it was determined that a ratio of 1% resulted in better efficiency compared to 0.5% and 2% ratios.

The effect of various design parameters such as incident wave height, orifice diameter, and pneumatic turbine efficiency on the hydrodynamic performance of an OWC has been investigated (Elhanafi et al., 2016). By defining dimensionless coefficients, they also evaluated the energy conversion process from wave energy to electrical power. The results showed that the wave reflection coefficient decreases as the turbine efficiency increases and the energy extraction coefficient increases.

In another study, a two-dimensional analysis on the performance of an OWC in OpenFOAM software was performed, focusing on geometric changes (Rezanejad et al., 2019). In this research, wave reflection and energy loss coefficients were studied. The energy loss coefficient depends on wave height, and as the period increases, the wave reflection coefficient decreases.

An OWC device's geometric parameters have been investigated to achieve the highest efficiency in wave conditions in the Faroe Island in the Persian Gulf, resulting in a 1.45% increase in system performance (Hayati et al., 2020). The draft depth and characteristics of the incident wave have been analyzed to evaluate the output power, velocity, and performance of the OWC under Caspian Sea wave conditions (Alizadeh Kharkeshi et al., 2020). This study found an increase in frequency from 0.5 to 0.7 Hz, which decreased output power.

The effect of wave frequency and draft depth on the performance of an OWC under Caspian Sea wave conditions (at a scale of 1:10) has been investigated, and it found that increasing the wave frequency leads to a decrease in the power and efficiency of the converter. The optimal non-dimensional draft is 0.24 (Alizadeh Kharkeshi et al., 2022). Additionally, through experimental testing of an OWC, it has been demonstrated that the presence of the OWC under Caspian Sea wave conditions leads to the occurrence of the sloshing phenomenon at high frequencies. Numerical study can be a valuable tool to analyze the hydrodynamic behavior of the converter at these frequencies (Kharkeshi et al., 2022a).

Studies in the field of OWCs indicate that the geometric parameters of the device significantly impact its performance. Among the geometric characteristics of the device, the front wall can be of great importance due to its direct interaction with the incident waves. In many past studies, changes in the front wall and the geometric conditions at the inlet of the OWC have been investigated.

Due to its suitable potential energy waves, the Caspian Sea was chosen for research. The existence of low-frequency waves with shorter wavelengths compared to open seas and oceans distinguishes the conditions of this sea.

Previous research in this sea has shown that increasing the frequency from 0.5 to 0.7 Hz causes a decrease in output power due to the occurrence of sloshing (Kharkeshi et al., 2023). In this study, the numerical change of the system's inlet height on its performance was initially investigated at a 1:10 scale concerning the conditions of the waves in the Caspian Sea and past research on OWCs. Then, to optimize the geometric parameters for achieving the best system performance and reducing wave sloshing at a frequency of 0.7 Hz and a period of 1.43 seconds, the effect of adding an inlet at angles ranging from 0 to 40 degrees with a 20-degree increment to the geometry was explored.

The geometry of this study was drawn and meshed, and modeled as three-dimensional, two-phase, and turbulent flow using the open-source software OpenFOAM.

This numerical study utilized the SST K-ω equations for turbulent conditions, Reynolds-averaged Navier-Stokes (RANS) equations for solving momentum and pressure equations, and the OlaFlow solver.

A moving wall boundary condition was employed to generate waves that are consistent with the conditions of the Caspian Sea. In contrast, a reflecting boundary condition was used to prevent wave reflections and simulate the coast.

To evaluate the results of simulating waves with a frequency of 0.7 Hz and a period of 1.43 seconds, the converter's hydrodynamic response was described using free surface oscillations, flow rate, and pressure measurements.

The impact of the inlet height and changes to the geometry of the OWC by adding an inlet on the hydrodynamic response, the energy balance coefficients, the investigation of the sloshing phenomenon, and the power were investigated. Finally, the appropriate geometry was determined using optimization results. This research was conducted to improve the system's performance and reduce the destructive effects caused by sloshing.

1.1 Target Sea

The following section outlines general (non-formatting) guidelines to follow. These guidelines are applicable to all authors and include information on the policies and practices relevant to the publication of your manuscript.

In order to analyze the performance of the fluctuating water column, the conditions appropriate to the Caspian Sea should be specified. By examining the wave energy potential of the Caspian Sea, it has been stated that the southern coast of the Caspian Sea, which is deeper than other areas of this sea, is suitable for installing wave energy converters (Alamian et al., 2017). According to the characteristics of the waves of this sea, such as the wave period from 0 to 8 seconds and the wave height from 0 to 2.5 meters, the research to generate energy from the waves of the Caspian Sea was expanded. According to the results, it was found that the waves in the period of 2 to 4 seconds and at the height of 0 to 0.5 meters have occupied the most hours throughout the year, and in the period of 4 to 6 seconds and height of 0.5 to 1 meter have the most energy.

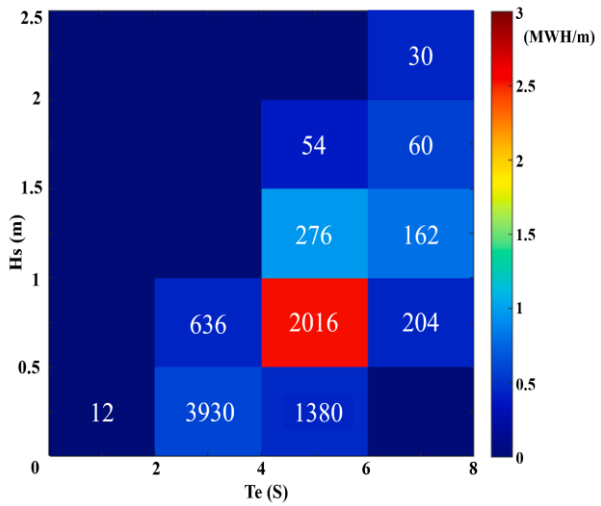

Fig. 1 Graph of the possibility of occurrence and energy density of waves according to the parameters of effective height and wave period for Babolsar (Alamian et al., 2017)

Table 1 Froud scaling

Wave characteristics	Unit	Scale Factor	Prototype	Lab
Period	s	$\alpha_l^{0.5}$	4-8	1.25-2.52
Height	m	α_l	0.5-1	0.05-0.1
Frequency	Hz	$\alpha_l^{-0.5}$	0.12-0.25	0.4-0.8

The Froud scaling technique has been utilized to replicate laboratory conditions for simulating waves in the Caspian Sea. The specifics of the target sea wave conditions are shown in Fig. 1.

1.2 Froud Number Scaling

The Froud number is one of the dimensionless numbers in fluid mechanics, which expresses the ratio of inertial force to gravity force in a fluid motion. In the oscillating water column energy converter, with the condition of establishing Froud number equality, the results of the scaled model can be considered the same as the results in real dimensions. The Froud number could be calculated from the following Equation:

$$Fr = \frac{V}{\sqrt{Lg}} \tag{1}$$

Scale factors for wave period, height, and frequency can be observed in Table 1. In scaling down, the frequency and wave height required in the flume can be calculated with equations (2) and (3) (Kharkeshi et al., 2022a).

$$\omega_{act} = \alpha_L^{-0.5}\omega_{lab} \tag{2}$$

$$\mathrm{H}_{act} = \alpha_L \mathrm{H}_{lab} \tag{3}$$

α_L is the scale factor, ω is the frequency and H is the wave height, and the act and lab subscripts are for actual and laboratory conditions, respectively (Kharkeshi et al., 2022c).

2. MODEL SETUP

Research on OWCs has been conducted in the sea-based Energy Group based on EMEC standards (Alizadeh Kharkeshi et al., 2020; Yazdi et al., 2020; Alizadeh Kharkeshi et al., 2021a; Kharkeshi et al., 2022a; Shafaghat et al., 2022). These studies show that the phenomenon of sloshing occurs when the OWC is exposed to the wave conditions of the Caspian Sea. To investigate this phenomenon, numerical analysis must be conducted on the converter. In this regard, an OWC was placed 5L away from the wave maker to investigate how changing its geometry improves performance in the present study. The investigation was conducted in two stages. First, the numerical analysis of the converter's performance was carried out by changing the height of the OWC inlet. Second, an inlet was added to the OWC, and the angle of the inlet walls was changed to improve performance and reduce the destructive effects of sloshing. The optimal condition for the OWC was determined. Figures 2 and 3 depict the changes in geometry in the two stages, and Table 2 presents the geometric specifications of the studied OWC.

The effect of changing the height of the oscillating column's front wall and placing an inlet with different angles to improve performance and reduce the sloshing phenomenon was investigated according to Table 3.

2.1 Numerical Study

In this study, the geometry of the OWC was drawn and meshed. The open-source software OpenFOAM was employed to model the interaction between waves and the OWC in the conditions of the Caspian Sea. This software works based on the finite volume method and uses RANS equations to solve for velocity and pressure. OlaFlow solver was used to simulate waves and the SST k-ω equations were used to model turbulence in the computational domain.

The open-source nature of OpenFOAM allows for better control of numerical solutions, and its specialized solvers for simulating waves, such as OlaFlow, with high accuracy and precision for simulating waves and their interaction with structures, were reasons for selecting this

Table 2 Dimensional specifications of the inlet

variable	icon	value (m)
Water depth	h	1-1.1
OWC length	a	1
OWC height	b	1.6
Outlet diameter	D	0.1
Inlet height	O	0.75-0.85
Draft depth	d	0.25
OWC width	L	1

Table 3 Dimensional specifications of the inlet

θ(deg)	0	20	40
X(m)	0	0.273	0.63

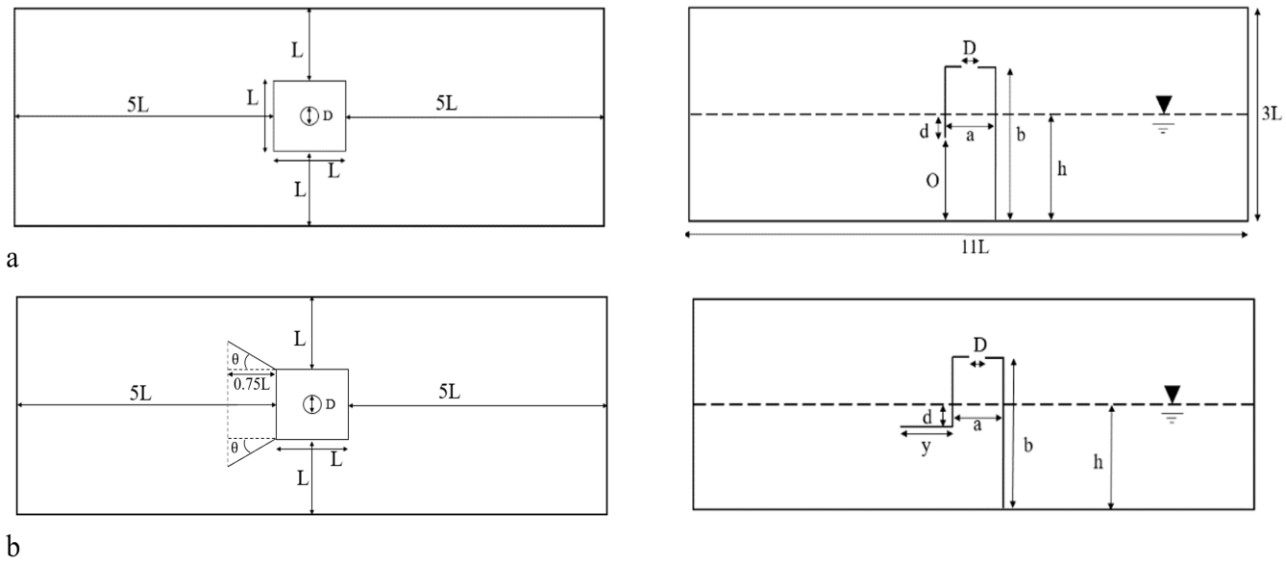

Fig. 2 Top and side view of a) an OWC without an inlet b) an OWC with an inlet

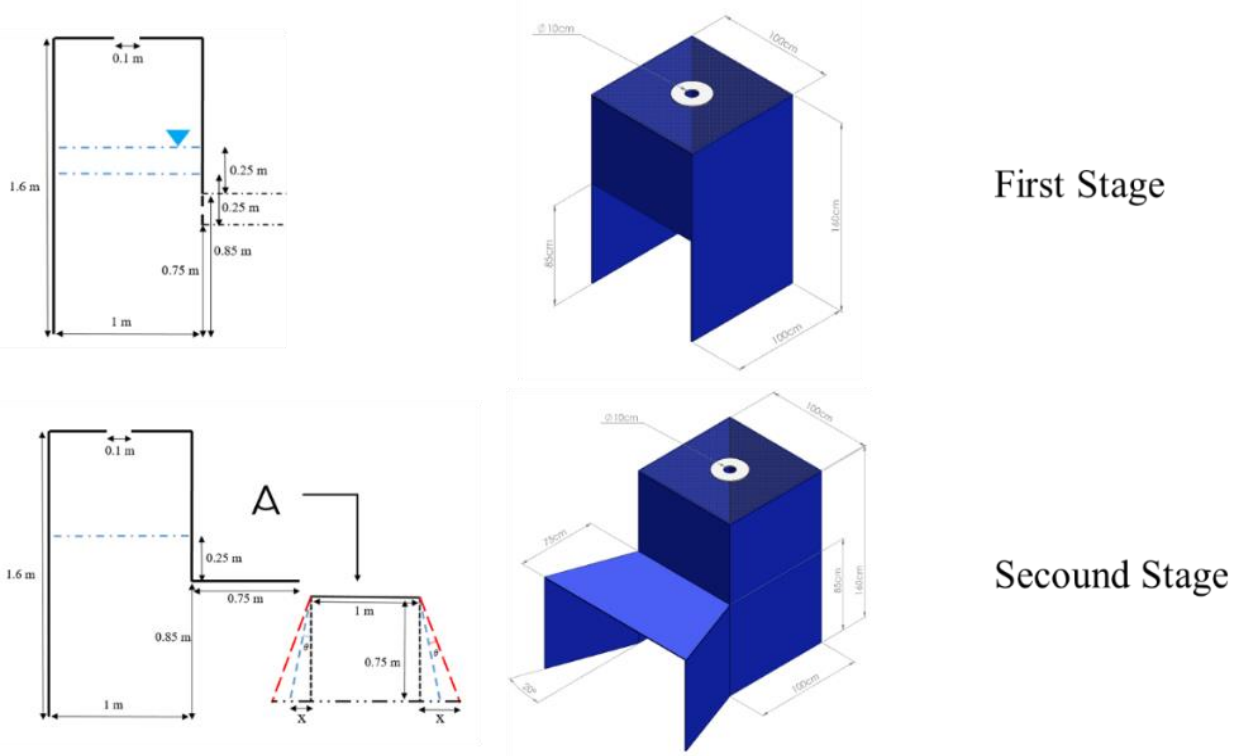

Fig. 3 Stages of changing the geometry of the oscillating water column to improve performance and reduce sloshing occurrence

software. After validating the numerical results with experimental data, the speed, free surface oscillations, and output power of the studied converter were studied.

2.2 Governing Equations

In this study, the governing equations were determined for a three-dimensional computational domain, considering two fluids (water and air) with constant density and non-compressible assumptions and considering the effect of viscosity. The RANS equations were used to numerically solve and calculate pressure variables within the OWC and the outlet air velocity from the orifice. To simulate turbulent conditions, the SST k-ω equations were employed. The software settings and governing equations used in the simulation are discussed in the following.

The governing equations are as follows:

2.2.1 Continuity and RANS

The continuity equation for incompressible flow is expressed as follows (López et al., 2014):

$$\frac{\partial u_i}{\partial x_i} = 0 \tag{4}$$

The momentum conservation equation is derived from Newton's second law. In transient and turbulent problems, time-averaged Navier-Stokes momentum

equations or Reynolds-averaged Navier-Stokes equations are used (López et al., 2014). The Reynolds stresses, unknowns in the equations, are modeled using a turbulence model.

$$\rho\frac{Du_i}{Dt} = -\frac{\partial P}{\partial x_i} + (\mu + \mu_t)\frac{\partial}{\partial x_j}\left(\frac{\partial u_i}{\partial x_j} + \frac{\partial u_j}{\partial x_i}\right) + f_i \quad (5)$$

In Eq. (4) and (5) (López et al., 2014), u_i represents the average velocity in the x, y, and z directions, t is time, P is pressure, f_i represents volumetric forces, ρ is density, μ is dynamic viscosity, and μ_t is the turbulence coefficient resulting from geometry.

2.2.2 Turbulence Model

Turbulence models such as k-ω and k-ε have simulated turbulent conditions in OWC problems. Kármán et al. (Kamath et al., 2015) investigated fifth-order Stokes nonlinear waves using the k-ω turbulence model, which showed good agreement between numerical and experimental results. However, it should be noted that the k-ε model does not perform well in flows with velocity decay and separation due to reverse pressure gradients. This study used the SST k-ω turbulence model, a combination of the k-ω and k-ε models. Since in this research, different areas close to the wall and outside it are important, and also because of the reverse pressure gradient, the SST K-ω model was used. The SST k-ω turbulence model operates based on two equations: the turbulence kinetic energy (K) equation and the turbulent dissipation rate (ω) equation, which are expressed as follows (Menter, 1994):

$$\frac{\partial \omega}{\partial t} + u_i\frac{\partial \omega}{\partial x_i} = \frac{\omega}{k}P_\tau - \beta\omega^2 + \frac{\partial}{\partial x_i}\left[\left(\mu + \sigma_\omega\frac{k}{\omega}\right)\frac{\partial \omega}{\partial x_j}\right] + \frac{\sigma_d}{\omega}\frac{\partial k}{\partial x_j}\frac{\partial \omega}{\partial x_j} \quad (6)$$

$$\frac{\partial k}{\partial t} + u_i\frac{\partial k}{\partial x_i} = P_\tau - \beta^*\omega k + \frac{\partial}{\partial x_j}\left[\left(\mu + \sigma_k\frac{k}{\omega}\right)\frac{\partial k}{\partial x_j}\right] \quad (7)$$

$$P_\tau = \tau_{i.j}\frac{\partial u_i}{\partial x_j} \quad (8)$$

In the given equations, P_τ represents the power generation of turbulent kinetic energy due to the shear stress, and the constants β and β^* are equal to 0.072 and 0.09, respectively. The values of σ_ω, σ_d, and σ_k are considered to be 0.5, 0.856, and 0.85, respectively.

2.2.3 Volume Fraction

Numerical solution and determination of free surface oscillations in the presence of two or more immiscible fluids differ from that of a single fluid. The volume of fluid (VOF) method was used to model the two-phase flow of air and water. In this method, each computational cell can contain water, air, or both; therefore, coefficients are used to determine the volume occupied by each fluid in each computational cell. f_1 represents the volume occupied by water and the sum of these coefficients is always equal to one. The volume fraction of the two fluids is obtained from Eq. (9) (López et al., 2014).

Each computational cell can be in one of three states in these types of problems. If f_1 represents the volume occupied by water, then if f_1 is zero, the cell is empty of water and entirely filled with air. If f_1 is one, the entire volume of the cell is occupied by water. If f_1 is a value between zero and one, the cell is at the interface between the two fluids, and the volume of the cell is divided into a portion of water (f_1) and a portion of air ($1 - f_1$).

$$\frac{\partial f_i}{\partial t} + u_j\frac{\partial f_i}{\partial x_j} = 0 \quad (9)$$

The index i in Eq. (9) is the numerator, with values 1 and 2 corresponding to water and air, respectively. In the free surface and contact of the two-phase water and air, the combined values of density and dynamic viscosity will depend on the relative volume of each fluid in the computational cell. They can be determined using the following relationships (López et al., 2014):

$$\mu = \mu_1 f_1 + \mu_2(1 - f_1) \quad (10)$$

$$\rho = \rho_1 f_1 + \rho_2(1 - f_1) \quad (11)$$

2.2.4 Wave Maker Boundary Condition

After determining the water height, suitable wave height, and wave number, the appropriate displacement value is determined using Eq. (12) for generating waves with the desired characteristics using the flap-type wave maker (Alizadeh Kharkeshi et al., 2020).

$$\Delta = H\frac{\sinh(2kh) + 2kh}{4sinh(kh)^2} \times \frac{1}{[1 + \frac{1 - \cosh(kh)}{kh\sinh(kh)}]} \quad (12)$$

In Eq. (12), h represents the water depth, H is the wave height, and k is the wave number.

2.2.5 Coastal Boundary Condition

The 2D active absorption method was used to simulate beach conditions, as used in (Schäffer & Klopman, 2000)'s article.

Shallow water theory offers great convenience due to the constant velocity along the height of the water column, aligning perfectly with the generation of waves using a piston-type wavemaker. Furthermore, this characteristic eliminates the occurrence of evanescent modes, as the velocity profile precisely represents the progressive wave component. Consequently, Equation (13) can be derived from this wave theory.

$$Uh = c\eta \quad (13)$$

The variable to solve for in this context is U, which represents the horizontal vertically-integrated (uniform) velocity, while c denotes the wave celerity. To obtain the value of U, measurements of h and η are necessary, which consequently requires estimating the wave celerity (c).

The magnitude of c can be calculated using Equation (15).

To achieve the damping of reflected waves, the boundary must generate a velocity that matches the incident velocity but in the opposite direction. By rearranging Equation (13) to associate the free surface with the reflected wave (denoted as η_R, the one intended for damping), we obtain the active wave absorption expression as depicted in Equation (14).

$$U_c = -\sqrt{\frac{g}{h}}\eta_R \tag{14}$$

The correction velocity, denoted as Uc, is applied to a vector perpendicular to the boundary and points into the domain. The reflected wave height represented as η_R, is determined by subtracting the measured elevation at the wavemaker (η_M) from the target elevation (η_T). This calculation follows the expected reflection-free wave generation principle, expressed as $\eta_R = \eta_M - \eta_T$.

This theory primarily focuses on two-dimensional results but can be readily extended to three dimensions. In cases where reflected waves propagate parallel to the wavemaker, the anticipated behavior remains consistent with the 2D scenario. However, if this is not the case, the absorption theory can be applied independently to each paddle of the wavemaker. This allows for efficient handling of situations where reflected waves deviate from parallel propagation (Higuera et al., 2013).

2.2.6 Wave Velocity, Power and Energy

The wave propagation speed and group velocity are calculated based on Eq. (15) and (16), respectively (Elhanafi et al., 2016). Calculating the group velocity is important because it allows us to determine the input energy to the system. Additionally, calculating the group velocity can determine the time it takes for the wave to reach the device. This will help identify the appropriate time for numerical calculations.

$$c = \sqrt{\frac{g}{k}\tanh(\mathrm{kh})} \tag{15}$$

$$c_g = \frac{c}{2}\left[1 + \frac{2kh}{\sinh(2kh)}\right] \tag{16}$$

In Eq. (15), g is the acceleration due to gravity, h is water depth, and k is wave number. Using Eq. (15) and (16), c is wave velocity and c_g is group velocity. To calculate the efficiency of an OWC converter, the incident regular wave power, based on the theory of the Airy wave, is first calculated using the following equations (Alizadeh Kharkeshi et al., 2021b). To calculate the incident wave power, the group velocity of the wave and the incident energy on the system must be determined. Then, the converter efficiency can be obtained by calculating the power that can be extracted from the OWC (Shafaghat et al., 2022).

$$\mathrm{E_I} = 0.5\rho_{\mathrm{water}}\mathrm{gA}^2\lambda \tag{17}$$

$$P_{wave} = \mathrm{E_I c_g} \tag{18}$$

In Eq. (17) and (18), $\mathrm{E_I}$ represents the energy input or collision energy to the water column oscillator, A is the amplitude of oscillations, and λ is the wavelength.

2.2.7 OWC Power and Efficiency

After the wave enters the chamber of the converter, the wave's energy causes the fluid column to move, increasing the air pressure inside the converter. This pressure difference between the inside and outside of the converter results in an oscillatory airflow. The greater the pressure difference and volumetric flow rate of the air, the higher the power of the OWC. The extractable power from the OWC can be calculated using the following formula (Bouali & Larbi, 2013):

$$P_{out} = \frac{1}{T}\int_0^T \Delta P(t)Q(t)dt \tag{19}$$

In Eq. (19), $\Delta P(t)$ represents the pressure difference inside and outside the chamber, and $Q(t)$ is the air flow rate. The efficiency of the OWC is calculated by the ratio of the extractable power to the incident wave power (Bouali & Larbi, 2013).

$$\varepsilon = \frac{P_{out}}{P_{wave}} \tag{20}$$

2.2.8 Free Surface Elevations and Sloshing

As the waves enter and exit the converter, the free surface inside the OWC chamber begins to oscillate. Sometimes these oscillations move in only one direction, without any angle relative to the horizon, and the fluid column behaves like a piston. Other times, the oscillations move in more than one direction and form an angle with the horizon, resulting in a linear or sloping free surface inside the converter. This phenomenon is called sloshing (Zhang et al., 2023). To investigate sloshing, the slope of the free surface at any given moment can be obtained by dividing the difference between the free surface oscillations at two points inside the converter by the distance between those points. This slope is defined using the parameter S, and the angle of this slope can be calculated using Eq. (21).

$$\mathrm{S} = \frac{\mathrm{Y_{G2}} - \mathrm{Y_{G1}}}{\Delta \mathrm{x}} \tag{21}$$

$$\alpha = \tan^{-1}(\mathrm{S}) \tag{22}$$

In Eq. (21), $\mathrm{Y_{G1}}$ and $\mathrm{Y_{G2}}$ are the water levels inside the oscillation column at two points where the wave gauges are located, with a distance of 0.15 meters from the front and back walls of the system, respectively. Moreover, the parameter Δx represents the distance between the two wave gauges inside the container. In Eq. (22), the parameter α represents the angle at the free surface inside the oscillation column forms with the horizontal line.

Another dimensionless parameter to compare different OWC states in the presence of an inlet at various angles is the volumetric flow rate. This dimensionless parameter is the ratio of the volume of water inside the inlet to the volume inside the converter in a stationary state.

$$\mathrm{V_{relative}} = \frac{\mathrm{V_{inlet}}}{\mathrm{V_{OWC}}} \tag{23}$$

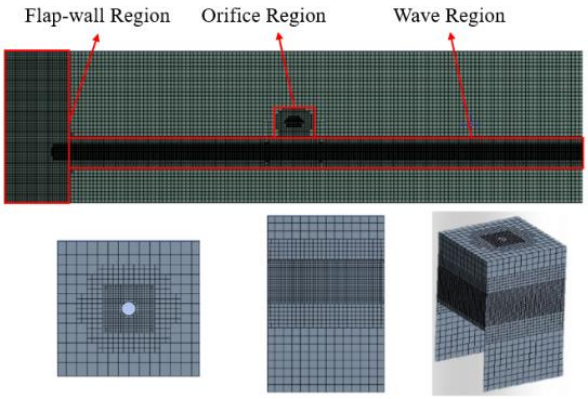

Fig. 4 Computational domain and the OWC mesh

2.3 Mesh and Time Step

Determining an appropriate time step is essential to ensure an accurate numerical solution. The value of the courant number, as the simulation software recommended, was 0.5. The Courant number is a dimensionless measure of simulation stability and convergence, equal to the product of velocity and time step divided by the length of the smallest grid cell. In this simulation, the time step is 0.02 seconds. The geometry of the OWC is investigated in two conditions: without an inlet and with a change in the height of the inlet, and then with the addition of an inlet to the geometry. In numerical modeling, the desired geometry and meshing are important, and a structured mesh has been used in this study. The grid includes 3,910,214 cells; the computational cost is equivalent to 3528 hours, or 147 days. The grid size is smaller in the free surface area due to wave formation, and in the initial area of the wave, flume to prevent negative cell volume as the wave maker moves as can be observed in Fig. 4. Since the turbulence of the numerical solution is considered, the skewness value, which is less than 0.85, is considered appropriate for the turbulent conditions. The dimensions of the simulation of the wave flume are 11 meters in length and 3 meters in width and height.

In this section, the boundary conditions are described. The boundary conditions were determined based on the Sea-based Energies lab wave flume. Accordingly, as can be observed in Fig. 5, the side walls and the floor of the wave flume were determined as non-slip walls. Since the top of the flume was connected to the surrounding environment, the pressure outlet boundary condition was specified. The wave flume was modeled using a flap-type wave maker to simulate shallow water waves. The wave maker plate was designed as a moving wall to create waves. The development of the code was based on the depth, period, and height of the waves, according to the characteristics of the Caspian Sea. The required course length for the desired wave generation is calculated by entering the input information, and the moving wall is created accordingly.

Wave reflection is critical in studying the performance of the OWC. The wave reflection creates two states, sometimes, the reflected wave adds positively to the incident wave and increases the height of the incident wave, and sometimes it creates a negative overlap and

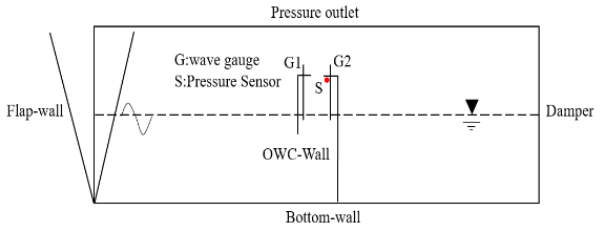

Fig. 5. Boundary conditions schematic

reduces the height of the incident wave. In both cases, the incident wave to the OWC is different from the intended wave, which results in errors and unacceptable results in evaluating the system's performance.

Wave reflections can have two effects on a system: first, after hitting the system and bouncing back, and second, after passing through the system and hitting the end of the flume. To prevent the effects of wave reflections in the first mode, the duration of numerical calculation and performance evaluation should be in a valid interval where the oscillations inside the chamber reach their maximum value until the oscillations suddenly decrease or increase. For the second section, a boundary condition is imposed to simulate coastal states, and a damper wall is installed at the end of the flume to prevent wave reflections. Finally, the surfaces of the OWC are determined in the form of the wall.

2.4 Genetic Algorithm

The most effective approach is to employ a genetic algorithm to optimize a general problem, like improving the geometric shape of a wave energy converter. Research has demonstrated that this method outperforms others, given the problem's specific conditions (Martinelli et al., 2013; Kharkeshi et al., 2022b). Genetic algorithms are search techniques used in computer science for approximating solutions to optimization and equation problems. John Holland initially introduced this algorithm, which relies on Darwin's principles of natural selection to determine the optimal formula for predicting or matching patterns. In the realm of artificial intelligence, the genetic algorithm (GA) serves as a problem-solving model, simulating genetic evolution as a means of programming.

The process of implementing genetic algorithms is as follows:

1. Chromosomes, representing potential solutions to the problem, are generated randomly to form the initial population.
2. A fitness function is introduced to evaluate the solutions, identifying promising candidates.
3. Selection operators are employed to choose better-performing chromosomes.
4. Reproduction operators are used to combine selected chromosomes and introduce mutations.
5. The current population merges with the new population resulting from the combination and mutation, creating a new generation of diverse chromosomes.

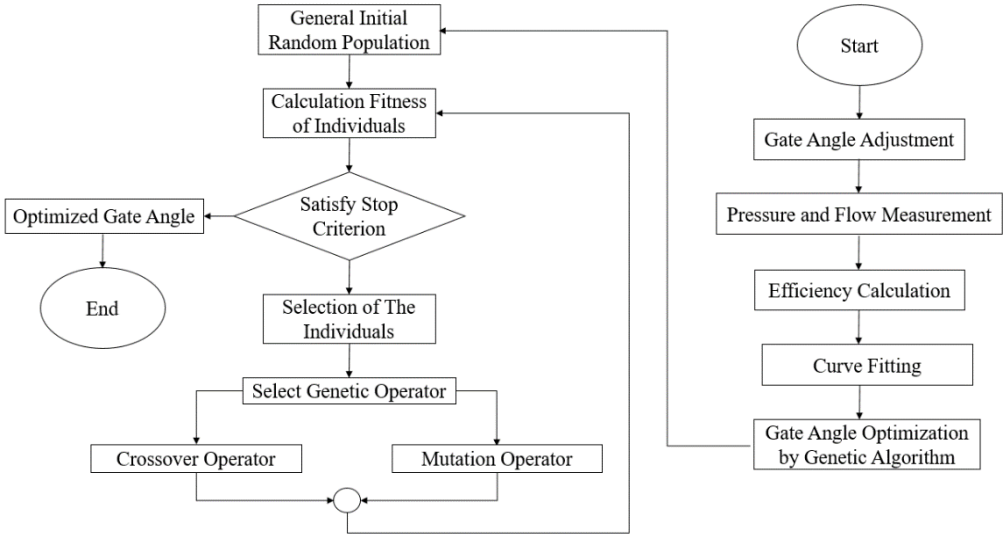

Fig. 6 Process of optimizing the inlet angle of the OWC flowchart using the genetic algorithm

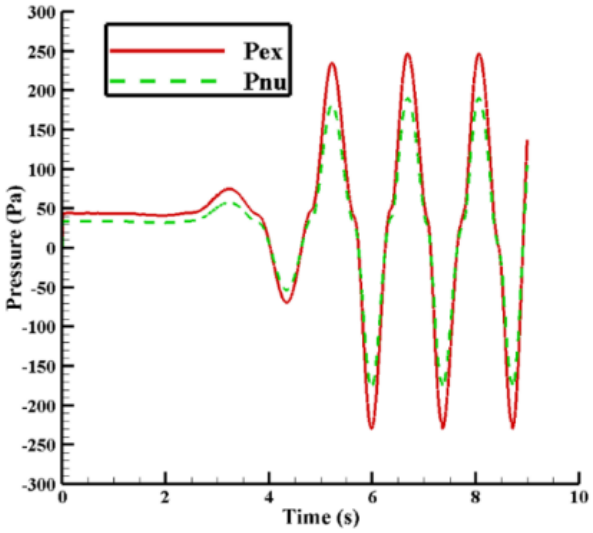

Fig. 7 Validation of the pressure inside the chamber. Pressure inside the chamber was calculated in the same spot as the experimental reference (x=7.4m, y=1.6m, z=1.5m)

6. The entire process is repeated for subsequent generations, selecting pairs for combination and generating new populations until the final stage is reached.

One of the various optimization techniques is the genetic algorithm, which is a type of evolutionary algorithm invented based on the laws of biology to find the optimal formula or values. The optimization was performed with two goals: reducing the destructive effects of sloshing inside the OWC and increasing the converter's efficiency. Initially, by fitting the curve of the numerical results of the system in the presence of an inlet, equations for the free surface oscillations in the system and the efficiency of the converter were extracted. Then, using the genetic algorithm, optimization was performed. After finding the optimal conditions, the geometry of the OWC with an inlet at the optimal angle was studied numerically. Fig. 6 depicts the genetic algorithm optimization flowchart. Finally, the genetic algorithm reached the optimal solution using 57 generations.

3. VALIDATION

A wave with a height of 0.149 m and a frequency of 0.7 Hz was generated using a moving wall as a wave-maker to validate the numerical results. The water depth was set to 1 m, resulting in a draft depth of 0.25 m. The numerical simulation used an OWC model with an inlet height of 0.75 m. In order to compare the numerical results with the experimental results, the pressure difference inside the OWC was extracted at a point where a pressure sensor had been installed in the experimental study, and then compared to the experimental pressure difference.

As can be observed in Fig. 7, the pressure variation plot obtained from both numerical and experimental analyses indicates a similar behavior between the two analysis methods. Hence, the results were validated through this comparison. By using the estimate of the normalization of the root mean square deviation or NRMSE error, the performance of the numerical model can be compared with the experimental results. For this purpose, the following relationship should be used (López et al., 2014).

$$\mathrm{NRMSE} = \frac{1}{\mathrm{x}_{max} - x_{min}} \left(\frac{1}{N}\sum_{i=1}^{N}(x_i - y_i)^2\right)^{\frac{1}{2}} \qquad (24)$$

where x_i are the values of the data measured in the physical model tests; y_i does the numerical model estimate the corresponding values; x_{max} and x_{min} are the maximum and minimum values of the physical model dataset. The results showed that the NRMSE error is equal to 7.2%.

After ensuring the accuracy and agreement of the numerical results with the experimental data, the

hydrodynamic response of the converter was evaluated by measuring the free surface oscillations, flow rate, and pressure. The effect of changes in the inlet height and the geometry of the OWC inlet with the addition of an inlet on the hydrodynamic response, hydrodynamic coefficients, energy balance coefficients, and power, were investigated. Moreover, the maximum energy dissipation occurring at the edges of the orifice was studied. Finally, an optimization was done to determine the optimal geometry based on the results.

4. RESULTS AND DISCUSSION

After validating the numerical results and ensuring their accuracy, a hydrodynamic study was conducted on an OWC to achieve two goals: reducing the destructive effects of sloshing and improving its performance and power. The results of the study of the OWC converter under the wave conditions of the Caspian Sea are presented in three stages:

1- Investigating the effect of the inlet height on the water column

2- Studying the effect of placing an inlet with different angles in front of the device

3- Optimizing the geometry of the converter using the genetic algorithm

In each stage of the study, the results are presented in three categories: hydrodynamic response, energy balance coefficients, and converter efficiency. The hydrodynamic response results include investigating the flow rate, pressure, and free surface oscillations.

4.1 Investigating the Effect of Inlet Height

When water flows back and forth in an OWC, it creates a difference in pressure between the air inside the converter and the surrounding environment. This pressure difference results in an alternating flow of air into and out of the converter chamber, creating a suction and discharge effect. The pressure difference created by the water flow depends on various factors such as the density of the water, the density and relative humidity of the air, the frequency and wavelength, as well as the geometry of the OWC. Changes in the geometry of the OWC will take various forms. Increasing the height of the water column inlet will increase the mass flow rate into the converter, increasing the efficiency of the OWC. The effect of this change on the hydrodynamic response, energy balance, and power of the converter will be evaluated.

4.1.1 Effect of Inlet Height on Flow Rate and Pressure

One of the important parameters in the performance of the OWC is the outlet velocity from the orifice, as increasing the outlet velocity leads to an increase in air flow rate, power, and efficiency of the OWC. According to the results obtained in Fig. 8, the increase in flow rate at the inlet height of 85 cm compared to 75 cm is observable throughout the solution time. This flow rate and pressure increase directly affects the system's output power and improves efficiency. The increase in pressure and flow rate is due to a rise in the inlet flow rate of water into the OWC, which means an increase in input energy to the system. Moreover, according to Fig. 9, the maximum velocity in the OWC increases with the inlet height of 85 cm compared to 75 cm.

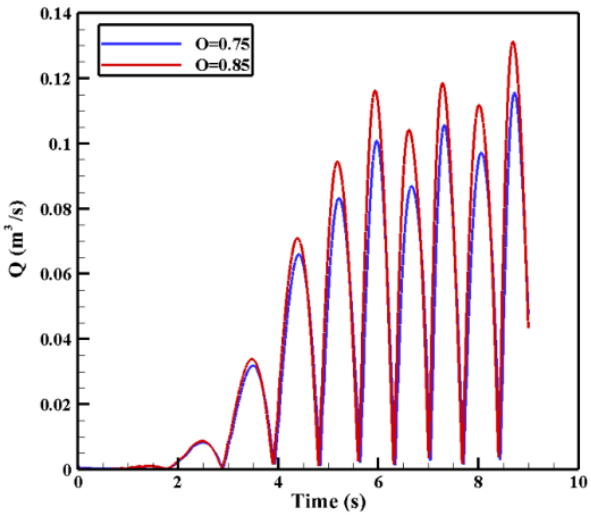

Fig. 8 Air flow throughout the orifice in inlet height of 75 cm and 85 cm

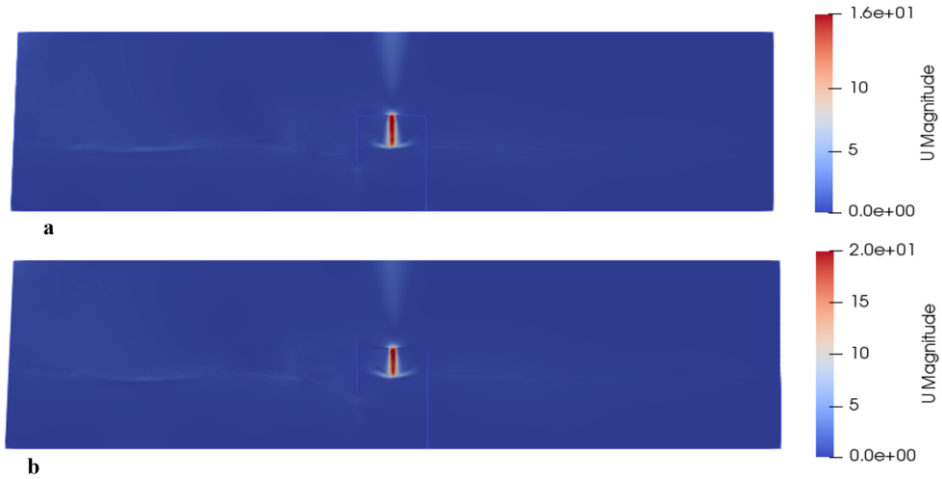

Fig. 9 Velocity distribution at 8.4 seconds at a) 75 cm inlet height, and b) 85 cm inlet height

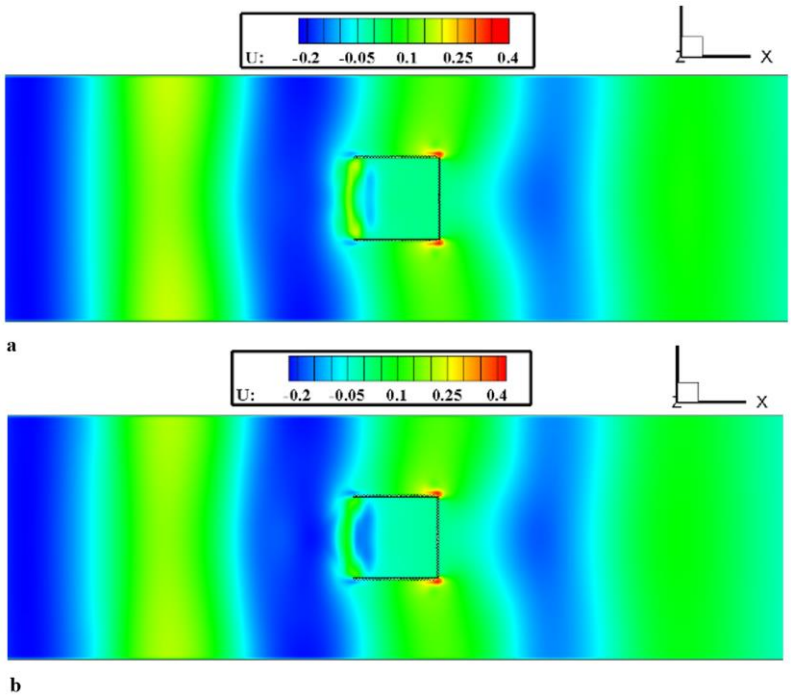

Fig. 10 Velocity distribution along the x-axis at 8.4 seconds and at the height of 10 cm below the inlet height a) inlet height of 75 cm b) inlet height of 85 cm

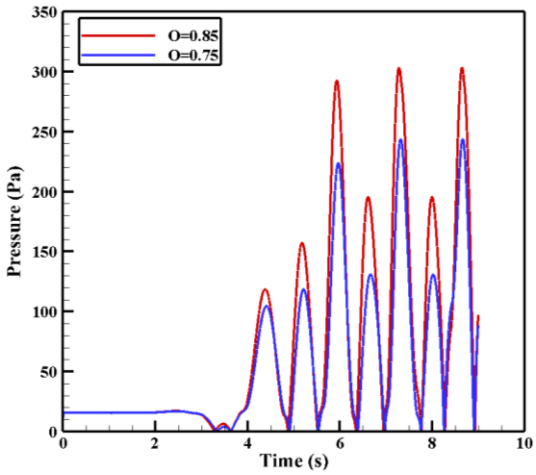

Fig. 11 Output pressure from OWC with inlet heights of 75 cm and 85 cm

Increasing the surface area of the inlet of the OWC will result in an increase in the inlet flow rate to the converter. However, as shown in Fig. 10, the velocity at the inlet at a height of 75 cm is 0.2 m/s, and at a height of 85 cm is 0.1 m/s. At the end edges of the converter, the velocity gradient and different directions of the two flows have created a vortex. In the vicinity of the inlet, a noticeable expansion in the velocity field area is observed at a height of 85 cm, concomitant with a decrease in velocity. This intriguing phenomenon can be attributed to the height increase of the inlet, which in turn leads to an augmented surface area. Consequently, as the inlet height rises, the inlet velocity diminishes, facilitating the fluid's entry into the chamber and, in effect, resulting in a more extensive velocity field area. Moreover, it is worth noting that all sections along the z-axis, positioned 10 cm below the inlet edge of the OWC, have been meticulously crafted and accounted for.

The output pressure from the orifice is a crucial parameter in examining the performance of the OWC converter. Figures 11 and 12 illustrate the fact that the output pressure parameter increases with the inlet height of the converter due to an increase in energy input to the system. Based on the orifice output pressure results, the pressure values for the entire study period in the OWC with an inlet height of 85 cm were higher than those in the OWC with an inlet height of 75 cm. The comparison of the maximum orifice output pressure values indicate a 16.6% increase in this parameter in the OWC with an inlet height of 85 cm. They were higher than those in the OWC with an inlet height of 75 cm. The comparison of the maximum orifice output pressure values indicates a 16.6% increase in this parameter in the OWC with an inlet height of 85 cm.

4.1.2 Effect of Inlet Height on Free Surface

The study investigated the oscillations of the free surface inside the water column with changes in the inlet height over a numerical solution period, as shown in Fig. 13. The results show that the entry of the first wave into the OWC has a low amplitude due to the inertia of the fluid column inside the chamber.

After the entry of subsequent waves, the amplitude of the oscillations increases. In addition to the geometry of the converter, the frequency of the waves also affects the free surface oscillations. The behavior of the free surface oscillations inside the OWC varies with the frequency of the waves. This behavior does not resemble the rigid piston theory in the conditions of the Caspian Sea waves, which have a high frequency. The turbulence of the free

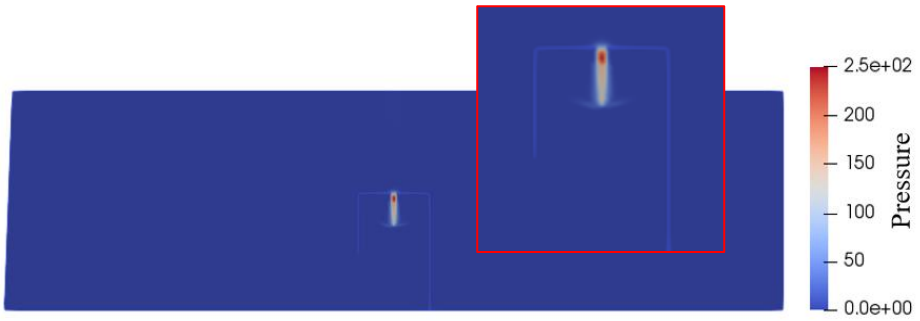

(a)

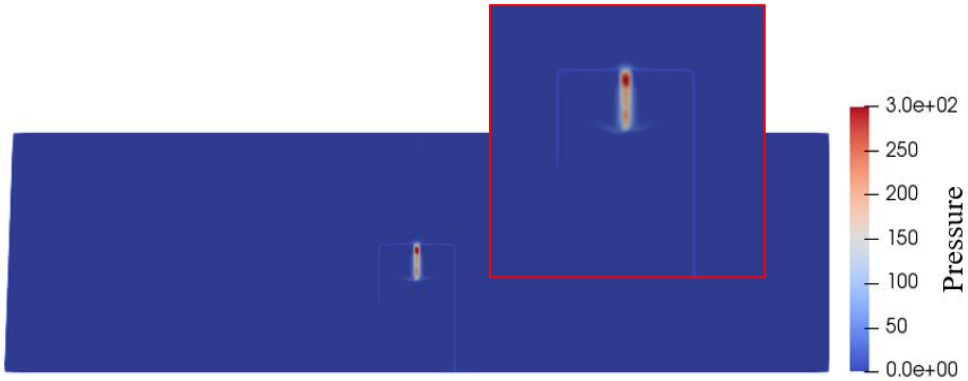

(b)

Fig. 12 Pressure distribution in orifice a) inlet height of 75 cm b) inlet height of 85 cm

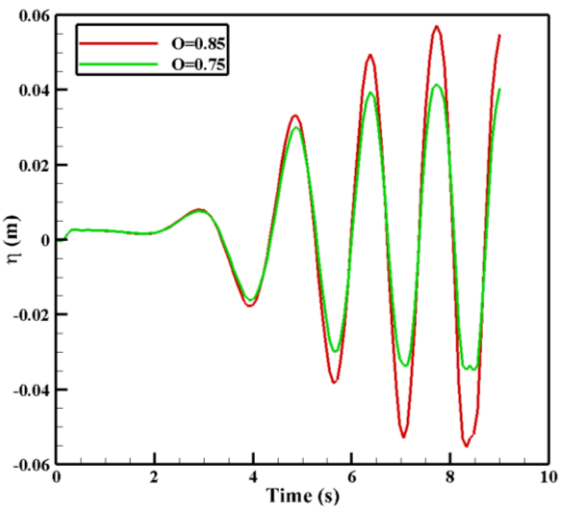

Fig. 13 Free surface oscillations for inlet heights of 75 cm and 85 cm

surface inside the water column is shown to have a linear or quadratic relationship with the frequency and geometry of the converter. The study investigates the type of oscillations and their impact on the performance of the OWC, using two oscillation sensors to calculate the oscillations and, consequently, the slope of the free surface.

After a wave collides with the front wall of an OWC (Figure 16 and 17), a high-pressure area with zero velocity is created in front of the converter. Due to this pressure difference and the flow separation from the front wall's edge, a vortex is formed in the water flow inside the converter's chamber. Studying the flow pattern at two heights of the inlet indicates that increasing the inlet height causes an increase in the vortex inside the chamber. Increasing the inlet height leads to a rise in the inflow rate and the vortex inside the chamber. The formation of the vortex is the result of the inlet edge; therefore, changing the inlet geometry that reduces the vortex inside the chamber can effectively improve the system's efficiency. Additionally, in the airflow, the pressure area inside the chamber and the separation from the two edges of the orifice create two vortices inside the chamber. The airflow in the 85 cm inlet height is more intense than in the 75 cm, because surface oscillation in 85 cm is higher than 75 cm and therefore velocity of the water free surface is higher and based on the continuity law air flow rate passing through orifice is higher (Fig. 13).

4.1.3 Effect of Inlet Height on OWC Efficiency

Analysis of various results obtained from changing the height of the inlet of an OWC show that such modifications lead to an increase in the maximum output power of the system and an improvement in the performance of the OWC. Furthermore, while the system's power increases and the lost energy coefficient decreases by raising the inlet height, the increase in free surface oscillations inside the OWC and the angle of the free surface with the horizon (as can be seen in Fig. 14) can cause destructive effects on the converter. To mitigate these effects, the next step of this research involves adding an inlet to the system with an inlet height of 85 centimeters, which aims to reduce the wave's destructive effects and increase the output power of the OWC.

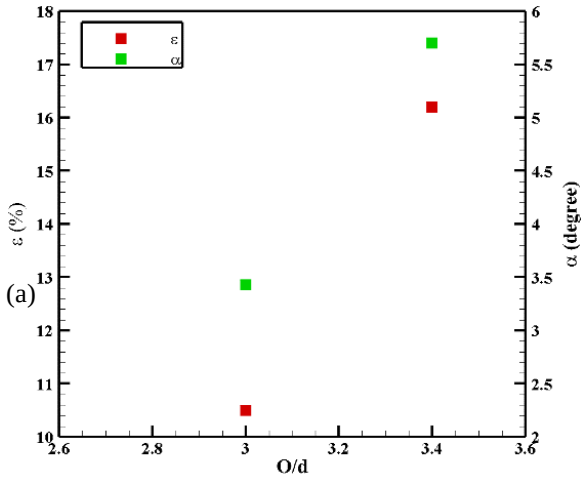

Fig. 14 Comparing the efficiency of OWC and angle of free surface inside the chamber forinlet heights of 75cm and 85 cm

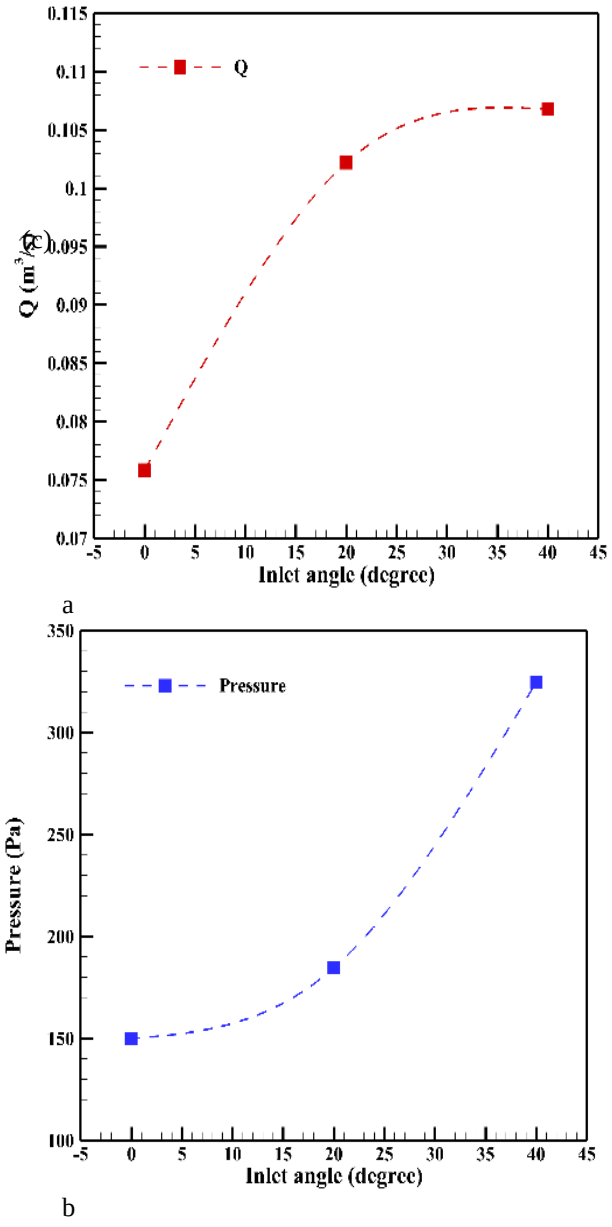

Fig. 15 Flow rate and output pressure from the orifice in different volume ratios

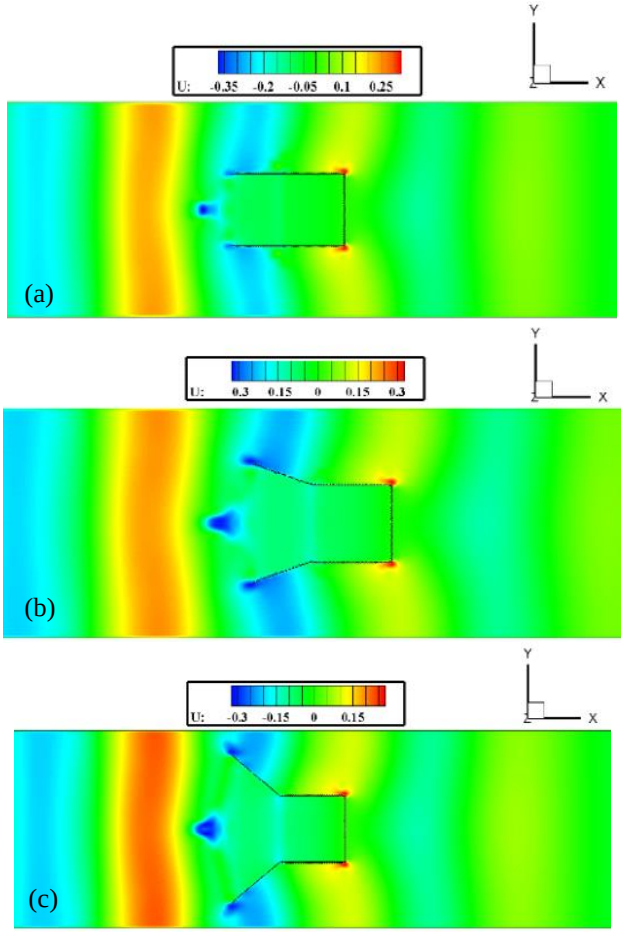

Fig. 16 Velocity distribution in the x direction at 8.4 seconds and at the height of 10 cm below the inlet height for: a) an OWC with a zero-degree angle inlet b) an OWC with a 20-degree angle inlet c) an OWC with a 40-degree angle inlet

4.2 Investigating the Effect of Inlet Duct

4.2.1 Effect of Inlet Duct on Flow Rate and Pressure

Both pressure and flow rate can increase effective output power. They are increasing flow rate increases output power by increasing the air velocity at the orifice. According to the results in Fig. 15, the airflow rate (mass flow rate) and pressure increased by 6.4% and 7.75%, at 40 degrees compared to 20 degrees, respectively. This velocity increase occurs when a more significant pressure difference is created between the inside of the chamber and the surrounding environment. Increasing the width of the inlet of the water column oscillation system results in an increase in the input energy to the design and, consequently, an increase in pressure inside the chamber and the output air flow rate. By examining the slope of the changes in pressure and airflow rate from the orifice in Fig. 15, it is clear that the slopes of these two parameters do not match. This discrepancy is due to the non-linear relationship between the two parameters. Therefore, changes in pressure will not necessarily correspond to changes in air flow rate.

Figure 16 illustrates velocity changes at the converter's entrance with an inlet. The placement of the inlet in front of the water column results in the inlet

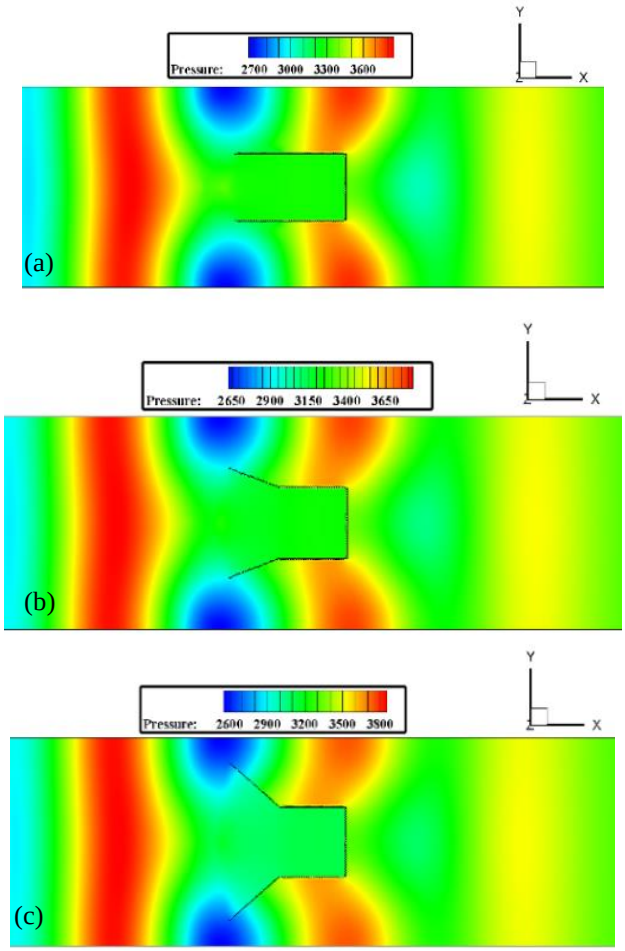

Fig. 17 Pressure distribution at 8.4 seconds and at the height of 10 cm below the inlet height for a) OWC with 0-degree angle inlet b) OWC with 20-degree angle inlet c) OWC with 40-degree angle inlet

behaving like a nozzle during wave entry and a diffuser during wave exit. Separation of the flow from the inlet wall and creating a low-pressure area leads to a decrease in velocity behind the inlet wall, which causes the flow to return.

As fluid flows through the edges of the OWC, the reduction in cross-sectional area and the effect of the convective term of acceleration on the velocity field lead to an increase in water flow velocity along the side walls of the OWC, resulting in a decrease in pressure (Fig. 17). One of the reasons for the more significant pressure drop in the side walls of the OWC with a larger angle inlet may be the existence of the non-slip boundary condition on the inlet wall, as shown in Fig. 17-c.

4.2.2 Effect of Inlet Duct on Free Surface

Free surface water oscillations have been investigated to evaluate the destructive effects of waves. The results in Fig. 18 indicate that, at different volume ratios, the free surface oscillations increase over time. However, it is essential to note that the increase in free surface oscillations inside the OWC with a 40-degree angle inlet compared to a 20-degree angle inlet has increased significantly. In fact, at its highest level, these oscillations have increased by 74.2 % more than the oscillations at the 20-degree angle.

Another critical point is that this increase has much less destructive effects than without the inlet. At a volume ratio of 0.94 or inlet angle of 40 degrees, the slope angle of free surface waves decreased by about 52.5% compared to the case without the inlet.

4.2.3 Effect of Inlet Duct on OWC Efficiency

After examining the results of the flow rate and pressure, which directly impact the power generated by the system, it was determined that increasing the angle of the inlet up to 40 degrees has increased the power generation, as can be seen in Fig. 19. This increase in power was 70.8% higher in the volume ratio of 0.83 compared to 0.74. Simultaneously an analysis of the efficiency results of the system and the free surface fluctuation angle reveals that, in addition to an increase in efficiency, an increase in the fluctuation angle occurs. However, it is worth noting that the oscillation angle at 40 degrees significantly decreases relative to the state without an inlet by an amount of 45.5 %.

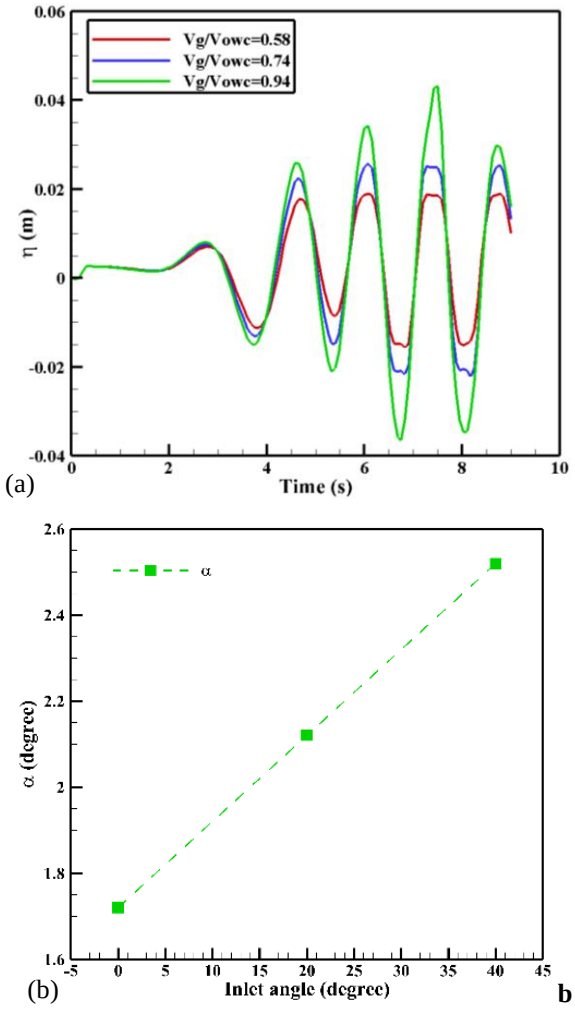

Fig. 18 a) Oscillations of the free surface and b) the slope angle of the free surface inside the OWC at different volume ratios

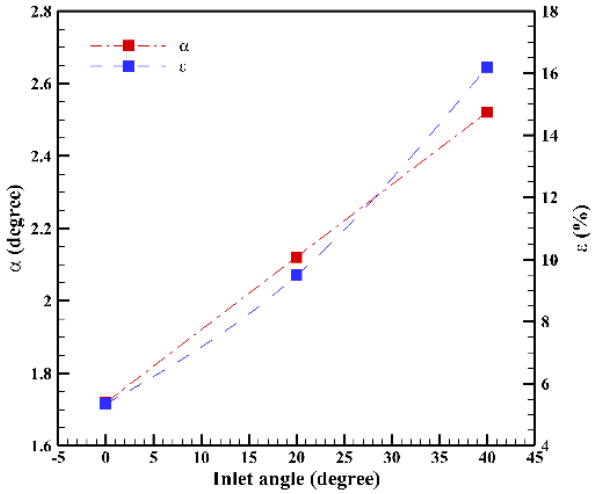

Fig. 19 Comparison of the maximum slope angle of free surface oscillations and OWC efficiency in different inlet modes

4.3 Optimization

After analyzing the results and identifying the improvement of the system's performance by increasing the inlet height and adding an inlet to the OWC, as well as reducing the free surface oscillations inside the water column, it is evident that changes in the geometry of the converter have led to system improvement. In the next step, a genetic algorithm was applied to fit the optimization curve and find the optimal output power from the device. The results indicate that the optimal point is at a volume ratio of 0.83 (with an inlet angle of 30 degrees).

4.3.1 Optimal System

The optimization results using the genetic algorithm indicate an optimal point in the OWC with a 30-degree angled inlet. Geometric optimization of the OWC was performed, and a numerical study on the converter with a 30-degree angled inlet was conducted. After analyzing the results in Fig. 20, it was determined that the angle of 30 degrees has the highest pressure and flow rate; therefore, the highest amount of power generation will occur at this angle.

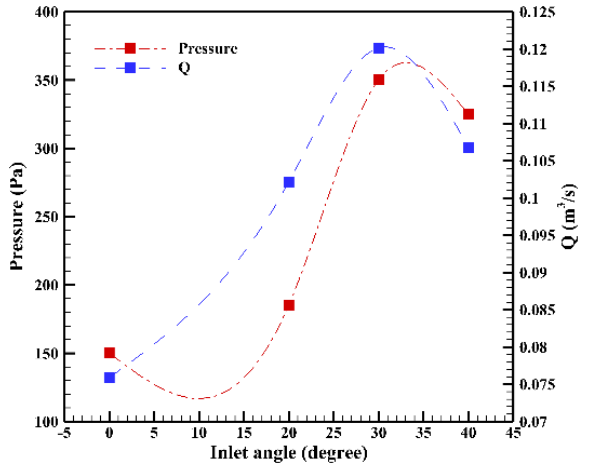

Fig. 20 Comparison of flow rate and pressure after optimization

Additionally, the pressure and velocity distribution at the inlet of the OWC was investigated in Fig. 21. The investigation of the pressure and velocity distribution near the flume wall and behind the inlet indicated a decrease in pressure due to the separation of the flow from the edge of the inlet wall. Moreover, velocity changes in this area will increase, and the negative velocity in this section is not due to a decrease in velocity behind the inlet wall, but due to a change in the flow direction in that area.

Figure 22 illustrates the system's performance alongside the slope angle after optimization. The inlet with a slope angle of 30-degrees has less sloshing than a 40-degree angle. The reduction in slope angle in the OWC with a 30-degree angled inlet compared to the inlet-less state is around 54%. This indicates that the goal of reducing the destructive effects of sloshing inside the chamber has been achieved. Furthermore, the results suggest that the OWC with a 30-degree angled inlet under the Caspian Sea wave conditions at a frequency of 0.7 Hz will generate the highest flow rate, pressure, power, and consequently, the highest efficiency.

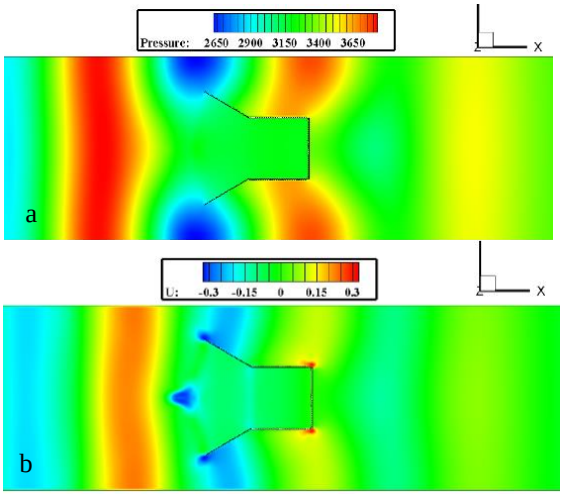

Fig. 21 OWC with an inlet at an angle of 30 degrees and at the height of 10 cm below the inlet height a) Pressure distribution b) Velocity distribution in the x direction

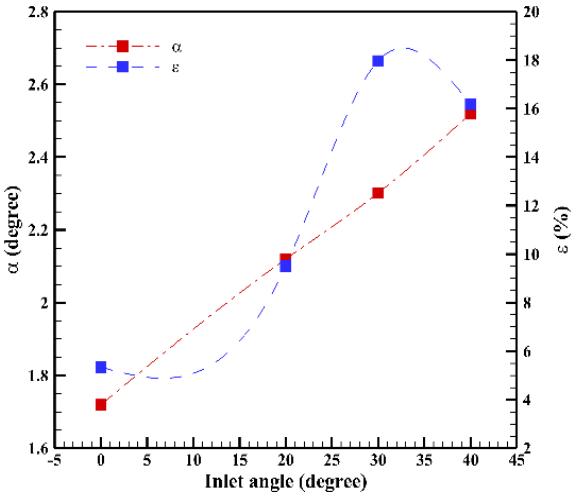

Fig. 22 Comparison of performance and angle of free surface oscillations inside OWC after optimization

5. CONCLUSION

Validation of the results based on experimental data and numerical simulations showed good agreement between them. Furthermore, the results indicated that increasing the height of the inlet by 10 centimeters led to an increase in efficiency from 10.5% to 16.2%, meaning a 13% increase in the height of the inlet resulted in a 54% improvement in system efficiency.

Regarding the hydrodynamic response of the system, changes in pressure, flow rate, and free surface oscillations can be noted. The results show that an increase in the inlet height can increase free surface oscillations by 38%, maximum pressure by 20%, and outlet flow rate by 13%.

After determining the improved performance with the increase in the height of the OWC inlet, an inlet was added to the system and its performance was evaluated at different volume ratios. The results of the outlet velocity from the orifice showed a 34.7% increase from 0 to 20 degrees, and a 6.4% increase from 20 to 40 degrees. Additionally, the pressure increased by 23.3% and 57.7% during changes in the inlet angle from 0 to 20 and 20 to 40 degrees, respectively.

By comparing the flow rate results and pressure in the presence of a 40-degree angle inlet and without an inlet at a height of 85 centimeters, it was determined that they have decreased by 8.22% and increased by 8.3%, respectively. Ultimately, the produced power in the presence of a 40-degree angle inlet at a height of 85 centimeters has become equal to the state without an inlet.

The study's results indicate a significant increase in the free surface oscillations at different volume ratios with time and at various angles. The highest increase of 74.2% in free surface oscillations inside the OWC occurred at an angle of 40 degrees compared to 20 degrees, where this oscillation increased by 33.4% when changing the angle from 0 to 20 degrees. Therefore, the increase in oscillations from 20 to 40 degrees was 45% higher than the oscillations from zero to 20 degrees, which can significantly increase destructive effects.

After optimization, the pressure and flow rate results indicate the presence of an optimum point at the 30 degrees inlet angle, where the efficiency of the OWC is 11% higher than at 40 degrees.

Increasing the height of the OWC inlet increased the OWC's performance efficiency, but it also increased the angle of the free surface inside the chamber. After adding an inlet to the OWC, the results were investigated and optimized at various angles. After optimization, it was determined that at a volume ratio of 0.83 (30-degree angle) and an inlet height of 85 centimeters, the free surface of the OWC decreased by 9.5% compared to a 40-degree angle inlet.

CONFLICT OF INTEREST

The authors have no conflicts to disclose

AUTHORS CONTRIBUTION

Seyed Sina Razavi: Numerical Study, Data Analysis, Visualization, discussion **Rouzbeh Shafaghat**: Supervisor, Discussion **Behrad Alizadeh Kharkeshi**: Post processing, Adviser, **Javad Eskandari:** Post processing, Writing- Reviewing and Editing

REFERENCES

Alamian, R., Shafaghat, R., Hosseini, S. S., & Zainali, A. (2017). Wave energy potential along the southern coast of the Caspian Sea. *International Journal of Marine Energy*, *19*, 221-234. https://doi.org/10.1016/j.ijome.2017.08.002

Alizadeh Kharkeshi, B., Shafaghat, R., Alamian, R., & Aghajani Afghan, A. H. (2020). Experimental & analytical hydrodynamic behavior investigation of an onshore OWC-WEC imposed to Caspian Sea wave conditions. *International Journal of Maritime Technology*, *14*, 1-12. http://dorl.net/dor/20.1001.1.23456000.2020.14.0.5.0

Alizadeh Kharkeshi, B., Shafaghat, R., Jahanian, O., & Alamian, R. (2021a). Experimental evaluation of the effect of dimensionless hydrodynamic coefficients on the performance of a multi-chamber oscillating water column converter in laboratory scale. *Modares Mechanical Engineering*, *21*(12), 823-834. http://dorl.net/dor/20.1001.1.10275940.1400.21.12.5.5

Alizadeh Kharkeshi, B., Shafaghat, R., Jahanian, O., Alamian, R., & Rezanejad, K. (2022). Experimental study on the performance of an oscillating water column by considering the interaction effects of optimal installation depth and dimensionless hydrodynamic coefficients for the Caspian Sea waves characteristics. *Ocean Engineering*, *256*, 111513. https://doi.org/https://doi.org/10.1016/j.oceaneng.2022.111513

Alizadeh Kharkeshi, B., Shafaghat, R., Jahanian, O., Rezanejad, k., & Alamian, R. (2021b). Experimental evaluation of the effect of dimensionless hydrodynamic coefficients on the performance of a multi-chamber oscillating water column converter in laboratory scale. *Modares Mechanical Engineering*, *21*(12), 823-834. http://mme.modares.ac.ir/article-15-52993-fa.html

Bouali, B., & Larbi, S. (2013). Contribution to the geometry optimization of an oscillating water column wave energy converter. *Energy Procedia*, *36*, 565-573. https://doi.org/10.1016/j.egypro.2013.07.065

Çelik, A., & Altunkaynak, A. (2020). Estimation of water column surface displacement of a fixed oscillating water column by simple mechanical model with determination of hydrodynamic parameters via physical experimental model. *Journal of Waterway, Port, Coastal, and Ocean Engineering*, *146*(5), 04020030. https://doi.org/10.1061/(ASCE)WW.1943-

5460.0000593

Delauré, Y., & Lewis, A. (2003). 3D hydrodynamic modelling of fixed oscillating water column wave power plant by a boundary element methods. *Ocean Engineering*, *30*(3), 309-330. https://doi.org/10.1016/S0029-8018(02)00032-X

Elhanafi, A., Fleming, A., Macfarlane, G., & Leong, Z. (2016). Numerical energy balance analysis for an onshore oscillating water column–wave energy converter. *Energy*, *116*, 539-557. https://doi.org/10.1016/j.energy.2016.09.118

Hayati, M., Nikseresht, A. H., & Haghighi, A. T. (2020). Sequential optimization of the geometrical parameters of an OWC device based on the specific wave characteristics. *Renewable Energy*, *161*, 386-394. https://doi.org/10.1016/j.renene.2020.07.073

Higuera, P., Lara, J. L., & Losada, I. J. (2013). Realistic wave generation and active wave absorption for Navier–Stokes models: Application to OpenFOAM®. *Coastal Engineering*, *71*, 102-118. https://doi.org/10.1016/j.coastaleng.2012.07.002

Horko, M. (2007). *CFD optimisation of an oscillating water column wave energy converter*. University of Western Australia. https://research-repository.uwa.edu.au/files/3236079/Horko_Michael_2007.pdf

Kamath, A., Bihs, H., & Arntsen, Ø. A. (2015). Numerical investigations of the hydrodynamics of an oscillating water column device. *Ocean Engineering*, 102, 40-50. https://doi.org/10.1016/j.oceaneng.2015.04.043

Kharkeshi, B. A., Shafaghat, R., Jahanian, O., Alamian, R., & Rezanejad, K. (2022a). Experimental study of an oscillating water column converter to optimize nonlinear PTO using genetic algorithm. *Energy*, 124925. https://doi.org/https://doi.org/10.1016/j.energy.2022.124925

Kharkeshi, B. A., Shafaghat, R., Jahanian, O., Alamian, R., & Rezanejad, K. (2022b). Experimental study of an oscillating water column converter to optimize nonlinear PTO using genetic algorithm. *Energy*, *260*, 124925. https://doi.org/https://doi.org/10.1016/j.energy.2022.124925

Kharkeshi, B. A., Shafaghat, R., Jahanian, O., Alamian, R., & Rezanejad, K. (2022c). Experimental study on the performance of an oscillating water column by considering the interaction effects of optimal installation depth and dimensionless hydrodynamic coefficients for the Caspian Sea waves characteristics. *Ocean Engineering*, *256*, 111513. https://doi.org/10.1016/j.oceaneng.2022.111513

Kharkeshi, B. A., Shafaghat, R., Rezanejad, K., & Alamian, R. (2023). Measuring and investigating the effect of sloshing on the performance of an OWC wave energy converter by means of a novel experimental approach. *Ocean Engineering*, *275*, 114130. https://doi.org/https://doi.org/10.1016/j.oceaneng.2023.114130

Liu, Z., Hyun, B.-S., Shi, H., & Hong, K. (2010). Practical simulation of oscillating water column chamber for wave energy conversion. *International Journal of Green Energy*, *7*(3), 337-346. https://doi.org/10.1080/15435071003796210

López, I., Pereiras, B., Castro, F., & Iglesias, G. (2014). Optimisation of turbine-induced damping for an OWC wave energy converter using a RANS–VOF numerical model. *Applied Energy*, *127*, 105-114. https://doi.org/10.1016/j.apenergy.2014.04.020

Mahnamfar, F., & Altunkaynak, A. (2017). Comparison of numerical and experimental analyses for optimizing the geometry of OWC systems. *Ocean Engineering*, *130*, 10-24. https://doi.org/10.1016/j.oceaneng.2016.11.054

Martinelli, L., Pezzutto, P., & Ruol, P. (2013). Experimentally based model to size the geometry of a new OWC device, with reference to the Mediterranean Sea wave environment. *Energies*, *6*(9), 4696-4720. https://doi.org/10.3390/en6094696

Menter, F. R. (1994). Two-equation eddy-viscosity turbulence models for engineering applications. *AIAA Journal*, *32*(8), 1598-1605. https://doi.org/10.2514/3.12149

Rezanejad, K., Bhattacharjee, J., & Soares, C. G. (2013). Stepped sea bottom effects on the efficiency of nearshore oscillating water column device. *Ocean Engineering*, *70*, 25-38. https://doi.org/10.1016/j.oceaneng.2013.05.029

Rezanejad, K., Gadelho, J., & Soares, C. G. (2019). Hydrodynamic analysis of an oscillating water column wave energy converter in the stepped bottom condition using CFD. *Renewable Energy*, *135*, 1241-1259. https://doi.org/10.1016/j.renene.2018.09.034

Schäffer, H. A., & Klopman, G. (2000). Review of multidirectional active wave absorption methods. *Journal of Waterway, Port, Coastal, and Ocean Engineering*, *126*(2), 88-97. https://doi.org/10.1061/(ASCE)0733-950X(2000)126:2(88)

Shafaghat, R., Fallahi, M., Alizadeh Kharkeshi, B., & Yousefifard, M. (2022). Experimental evaluation of the effect of incident wave frequency on the performance of a dual-chamber oscillating water columns considering resonance phenomenon occurrence. *Iranian (Iranica) Journal of Energy & Environment*, *13*(2), 98-110. https://doi.org/10.5829/ijee.2022.13.02.01

Simonetti, I., Cappietti, L., El Safti, H., & Oumeraci, H. (2015). *Numerical modelling of fixed oscillating water column wave energy conversion devices: toward geometry hydraulic optimization.* ASME 2015 34th International Conference on Ocean, Offshore and Arctic Engineering, https://doi.org/10.1115/OMAE2015-42056

Teixeira, P. R., Davyt, D. P., Didier, E., & Ramalhais, R.

(2013). Numerical simulation of an oscillating water column device using a code based on Navier–Stokes equations. *Energy*, *61*, 513-530. https://doi.org/10.1016/j.energy.2013.08.062

Yazdi, H., Shafaghat, R., & Alamian, R. (2020). Experimental assessment of a fixed on-shore oscillating water column device: Case study on oman sea. *International Journal of Engineering*, *33*(3), 494-504. https://doi.org/10.5829/IJE.2020.33.03C.14

Zhang, C., Dai, J., Cui, L., & Ning, D. (2023). Experimental study of nonlinear states of oscillating water column in waves. *Physics of Fluids*, *35*(1), 017108. https://doi.org/10.1063/5.0129191

Zhang, Y., Zou, Q. P., & Greaves, D. (2012). Air–water two-phase flow modelling of hydrodynamic performance of an oscillating water column device. *Renewable Energy*, *41*, 159-170. https://doi.org/10.1016/j.renene.2011.10.011